



On the separate treatment of mixing and spreading by the reactive-particle-tracking algorithm: An example of accurate upscaling of reactive Poiseuille flow

David A. Benson^{a,*}, Stephen Pankavich^b, Diogo Bolster^c

^a Hydrologic Science and Engineering, Colorado School of Mines, Golden, CO, 80401, USA

^b Department of Applied Mathematics and Statistics, Colorado School of Mines, Golden, CO, 80401, USA

^c Department of Civil and Environmental Engineering and Earth Sciences, University of Notre Dame, Notre Dame, IN, 46556, USA



ARTICLE INFO

Keywords:

Particle methods
Diffusion-reaction equation
Advection-diffusion-reaction equation
Numerical methods

ABSTRACT

The Eulerian advection-dispersion-reaction equation (ADRE) suffers the well-known scale-effect of reduced apparent reaction rates between chemically dissimilar fluids at larger scales (or dimensional averaging). The dispersion tensor in the ADRE must equally and simultaneously account for both solute mixing and spreading. Recent reactive-particle-tracking (RPT) algorithms can, by separate mechanisms, simulate 1) smaller-scale mixing by inter-particle mass transfer, and 2) mass spreading by traditional random walks. To test the supposition that the RPT can accurately track these separate mechanisms, we upscale reactive transport in Hagen-Poiseuille flow between two plates. The simple upscaled 1-D RPT model with one velocity value, an upscaled Taylor macro-dispersivity, and the local molecular diffusion coefficient matches the results obtained from a detailed 2-D model with fully described velocity and diffusion. Both models use the same thermodynamic reaction rate, because the rate is not forced to absorb the loss of information upon upscaling. Analytic and semi-analytic upscaling is also performed using volume averaging and ensemble streamtube techniques. Volume averaging does not perform as well as the RPT, while the streamtube approach (using an effective dispersion coefficient along with macro-dispersion) performs almost exactly the same as RPT.

1. Introduction

A recent improvement of the reactive-particle-tracking (RPT) method allows mass transfer between particles and subsequent reactions between any number of chemical constituents on the particles (Benson and Bolster, 2016). One of the features of this algorithm is that inter-particle mixing occurs separately from dispersive random walks. True mixing between dissimilar fluids usually occurs on smaller scales and at slower rates than the dispersive spreading (Cirpka and Kitanidis, 2000b; Danckwerts, 1953; De Simoni et al., 2005; Dentz et al., 2011; Dentz and Carrera, 2007; Ding et al., 2017; Donado et al., 2009; Hill, 1976; Le Borgne et al., 2013; Le Borgne et al., 2014; Lehwald et al., 2012; Molz and Widdowson, 1988; Nauman and Buffham, 1983; Rezaei et al., 2005). Schmidt et al. (2018a) suggested that the separate simulation of mixing and spreading by the RPT method could provide a way to accurately upscale reactive solute transport, because the smaller-scale true mixing dictates reaction rates, while the random walks simulate the process of particle separation that accompanies sub-grid (upscaled) velocity perturbations. Recent work has further extended the particle methods to

allow fluid/solid interaction (Schmidt et al., 2018b). For additional reasons, such as surface area scaling and solubility saturations near mineral grains, dissolution/precipitation reactions also suffer significant scaling effects of reaction rates (see Brantley et al., 2008; White and Peterson, 1990).

Two of the classic examinations of the disparity between mixing and spreading in moving fluids (and the effect on global reaction rates) were performed by Kapoor et al. (1997, 1998). These authors chose a simple system because it can be completely defined at the pore scale: laminar miscible displacement of chemically distinct (and reactive) fluids in Hagen-Poiseuille flow, either in a tube or between plates. In these cases, transport is exactly known, with the well-known parabolic velocity profile between no-slip walls, and random motion solely by molecular diffusion. The higher velocities at the center of the tube cause overlap of the fluids when projected to 1-D, but mixing only occurs along the warped interface. This system exemplifies the lag of mixing behind spreading in non-uniform velocity fields.

The spreading rate was first derived for Poiseuille flow by Taylor (1953), who showed that the 2-D transport of nonreactive tracer

* Corresponding author.

E-mail address: dbenson@mines.edu (D.A. Benson).

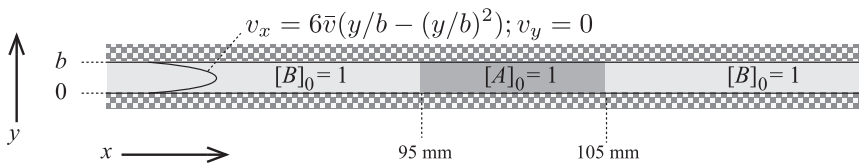


Fig. 1. Schematic of physical setup and initial condition. Not to scale.

in a tube could be upscaled (averaged) to 1-D. Given enough time to sample the entire velocity variability by local diffusion, transport can be effectively described by a one-dimensional advection-dispersion equation with constant velocity and an enhanced macro-dispersion coefficient reflecting subscale advection-induced spreading. The asymptotic ($t \rightarrow \infty$) upscaled longitudinal hydrodynamic macro-dispersion coefficient D_{mac} may be orders-of-magnitude larger than the local-scale molecular diffusion coefficient D_{mol} , and its functional form depends on the shear velocity distribution and molecular diffusion coefficient (e.g., Bolster et al., 2011).

This has inspired two tacks for upscaled reactive transport. The first tack has derived two dispersion coefficients, one for the effective mixing D_{eff} and another corresponding to Taylor’s D_{mac} that describes macro-dispersive spreading. In this approach, mixing is assumed to be the dominant mechanism dictating reaction rates (i.e., reactions are nearly instantaneous) so that the statistics of mixing via destruction of concentration gradients give an effective, smaller, dispersion coefficient (Cirpka and Kitanidis, 2000a, 2000b; Dentz and Carrera, 2007; Dentz et al., 2000). This smaller D_{eff} is designed to slow down reactions, but not place solutes in the correct locations, so Cirpka and Kitanidis (2000a) suggests a streamtube approach in which the spreading of the centers of mass for the streamtubes is given by D_{mac} , while mixing within a streamtube is given by the smaller D_{eff} . The second tack seeks to adjust the reaction rate itself by recognizing that the reactant segregation that results from upscaling should modify the effective reaction rate. This approach has been used on simpler (diffusion-only) problems that allow direct calculation of segregation—as measured by reactant concentration covariance evolution equations (Bolster et al., 2012; Paster et al., 2014; Schmidt et al., 2017; Tartakovsky et al., 2012). However, in heterogeneous velocity distributions, these equations have yet to be analytically solved, and only simpler expressions based on very fast or very slow reactions end-members have been developed (Porta et al., 2012).

These upscaling approaches point out the fundamental problem associated with an Eulerian advection, dispersion, and reaction equation (ADRE). The dispersion coefficient valid for conservative transport at

some scale will over-predict fluid mixing and reaction at the same scale, but under-predict spreading at some larger scale (or volume averaged to fewer spatial dimensions). We seek to correct this problem with a Lagrangian framework. For M species undergoing Fickian dispersion in incompressible flow, the coupled ADREs are

$$\frac{\partial c_i}{\partial t} = -\mathbf{v} \cdot \nabla c_i + \nabla \cdot (\mathbf{D} \nabla c_i) + R(c_A, c_B, \dots, c_M, k_1, \dots, k_N); \quad i = A, B, \dots, M \quad (1)$$

where c_i is the concentration of each of the species labeled $i = A, B, \dots, M$, \mathbf{v} is a velocity vector, \mathbf{D} is a dispersion tensor, and $R()$ is a reaction function among the M constituents with N reaction channels. The ADRE assumes that \mathbf{D} describes mixing and spreading in exactly the same way. For continuously varying \mathbf{v} , this is only true at the molecular scale. In practice, however, all variables and parameters in (1) have some finite support scale, and the discrepancy between mixing and spreading grows with support scale (Dentz et al., 2011; Le Borgne et al., 2013; Le Borgne et al., 2014). Indeed, if \mathbf{v} is given by Darcy’s Law and a hydraulic conductivity parameter, then this type of upscaling has already occurred. As briefly reviewed above, this discrepancy may be accounted for by adjusting the only remaining equation parameters that are held in the reaction term $R()$, or by solving the equation separately with larger and smaller \mathbf{D} to figure out mixing versus proper positions of reactants. If the perturbations of c_i , \mathbf{v} , and \mathbf{D} are known, as well as their auto- and cross-correlations in time and space, then the adjusted $R()$ can be approximated with closure assumptions (Dentz et al., 2011; Porta et al., 2013, 2012; Tartakovsky et al., 2012) that may not be particularly accurate for some values of coefficients. We include a brief comparison of the two most notable analytic upscaling approximations to our numerical method in this paper.

On the other hand, the micro-scale physics of particle motion and interaction may already carry all information neglected by the analytic upscaling. Here we show that, for the simplest case, the RPT method does indeed automatically track the necessary small-scale information and performs a natural upscaling.

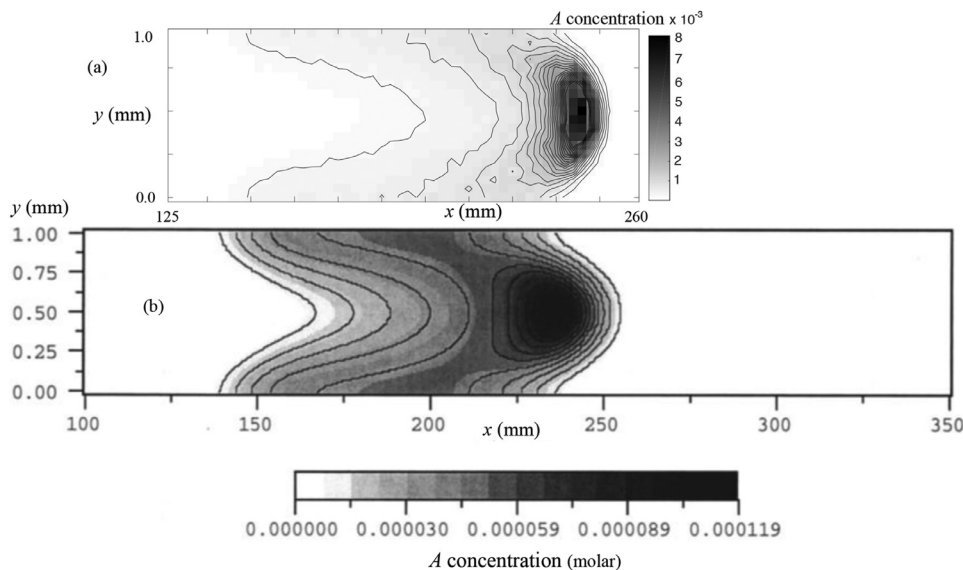


Fig. 2. 2-D maps of reactant A concentration after $t_D = 0.1$ ($t = 100$ s): a) Using RPT method (Bolster et al., 2016), and b) using finite-differences (reproduced from Kapoor et al. (1997)). Initial slug of A at unit concentration placed at $95 \leq x \leq 105$ mm. Contour interval in (a) is 2.5×10^{-4} molar. Note the sharper gradients and much higher concentrations (maximum approximately 70 times) maintained by RPT method.

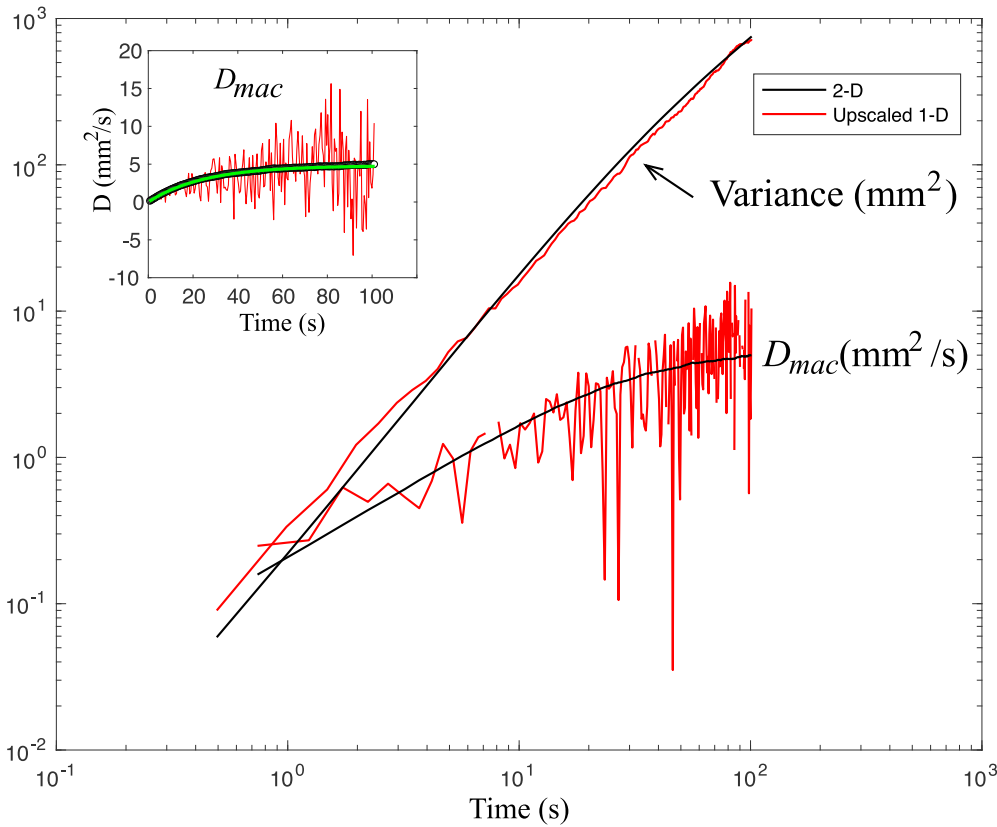


Fig. 3. Log-log plot of A particle variance and D_{mac} estimation from both 2-D and up-scaled 1-D models. The exponential model (green curve, inset) is shown against 2-D model (red) and 1-D posterior model results using the exponential. The 1-D model variance and posterior D show noise due to the smaller number of A particles (447). (For interpretation of the references to colour in this figure legend, the reader is referred to the web version of this article.)

2. Hagen-Poiseuille flow

We simulate an identical problem of flow, transport, and kinetic bimolecular reaction $A + B \rightarrow C$ between two parallel plates as did Kapoor et al. (1997) (Fig. 1). The concentration units are arbitrary, but we will use moles/L (molar). The local thermodynamic reaction rate is given by the law of mass action $R = -kc_A c_B$ for constituents A and B , where k [molar $^{-1}$ T $^{-1}$] is a rate coefficient. Without loss of generality we assume unit activity coefficients. This type of reaction has been studied experimentally and theoretically because of its simplicity and dependence on local mixing (e.g., Ding et al., 2012; Ederly et al., 2009; Ederly et al., 2010; Gramling et al., 2002; Raje and Kapoor, 2000; Sánchez-Vila et al., 2010; Zhang and Papelis, 2011). The plates are separated by aperture $b = 1$ mm, and the molecular diffusion coefficient is 10^{-3} mm 2 /s. An initial slug of reactant A is placed across the entire aperture from $x = 95$ to $x = 105$ mm (zero elsewhere), while reactant B is placed (with unlimited extent) only on either side of the slug. The velocity field follows $\mathbf{v} = [v_x(y), 0]$, where $v_x(y) = 6\bar{v}\left(\frac{y}{b} - \left(\frac{y}{b}\right)^2\right)$. The mean velocity is specified as $\bar{v} = 1.0132$ mm/s, giving a characteristic advection time of $t_a = b/\bar{v} = 0.99$ s. Kapoor et al. define an effective diffusion time $t_D = (b/\pi)^2/D_{mol}$ different from more recent definitions of $t_D = b^2/D_{mol}$ (e.g., Porta et al., 2012), so their Peclet and Damkohler numbers (100 and 10, respectively) are “off” by a factor of $\pi^2 \approx 10$. Our Peclet number is defined by $t_D/t_a = \bar{v}b/D_{mol} = 1013$. Kapoor et al. chose a reaction rate coefficient $k = 0.0987$ (Mol s $^{-1}$) to yield a Damkohler number of $Da = kc_A(t=0)b^2/D_{mol} = 98.7$, where the initial nonzero reactant concentrations are $c_A = c_B = 1$ molar.

First, we construct a 2-D simulation of the system using the particle-number-preserving method (Bolster et al., 2016). This is an extension of the original RPT algorithm that killed entire particles on reaction (see Benson and Meerschaert, 2008). The newer algorithm makes each particle carry only one species, and the mass (and concentration given a particle support volume) on that particle is continuously adjusted to ac-

count for reactions. We chose this method because the reactions are independent of the particle random walks, and we need to accurately track the variance of particle positions to validate upscaling to 1-D. Increasing particle numbers until convergence showed that 20,000 A particles and 240,000 total B particles in two 60 mm zones on either side of the initial A slug were sufficient. A gray-scale plot of the binned concentrations of A remaining at $t_D = 0.1$ ($t = 100$ s) shows the segregation of reactants that results from the parabolic velocity profile (Fig. 2a). Kapoor et al. used centered finite-differences in their solution, with a maximum grid Peclet number of $v_{max}\Delta x/D_{mol} = 37.5$, so that their solution was vastly artificially over-mixed (and over-reacted). Their peak concentrations of remaining reactant A are about 70 times less than ours, but the general shapes agree quite well. If one wished to use a first-order accurate (similar to Kapoor et al. (1997)) finite-difference method with a grid Peclet number on the order of unity, then $\Delta x \approx 1.7 \times 10^{-4}$. Using 100 nodes in the y -direction, the 200 mm \times 1 mm domain would require on the order of 120 million nodes. A more accurate advection scheme would require fewer nodes but would still be computationally demanding so we use the particle method for the benchmark 2-D simulations (see Benson et al., 2017 for a comparison of methods).

The RPT algorithm of Bolster et al. (2016) was used because individual particles are composed solely of A , B , or C . This allows us to track all A particles in the initial slug to verify the analytically upscaled value of $D_{mac}(t)$ (derived in the Appendix). The centered second moment (i.e., the “plume variance”) grows as expected (Fig. 3): quadratically near $t = 0$ because of ballistic particle motion according to the velocity profile, transitioning to linear growth according to Fick’s law. We took first differences in discretized time to calculate $D_{mac}(t) \approx \Delta \text{VAR}(X_A)/(2\Delta t)$. We fit $D_{mac}(t) = 4.88 \frac{\text{mm}^2}{\text{s}} [1 - \exp(-t/25\text{s})]$ for the upscaled (1-D) model from the 2-D data. Note that the analytic $D_{mac}(t)$ is almost exactly equal to our measured $D_{mac}(t)$ (see Appendix).

The locally well-mixed 2-D model used a particle density of 2,000/mm 2 , or a 2-D volume per particle of 5×10^{-4} mm 2 . An equivalent

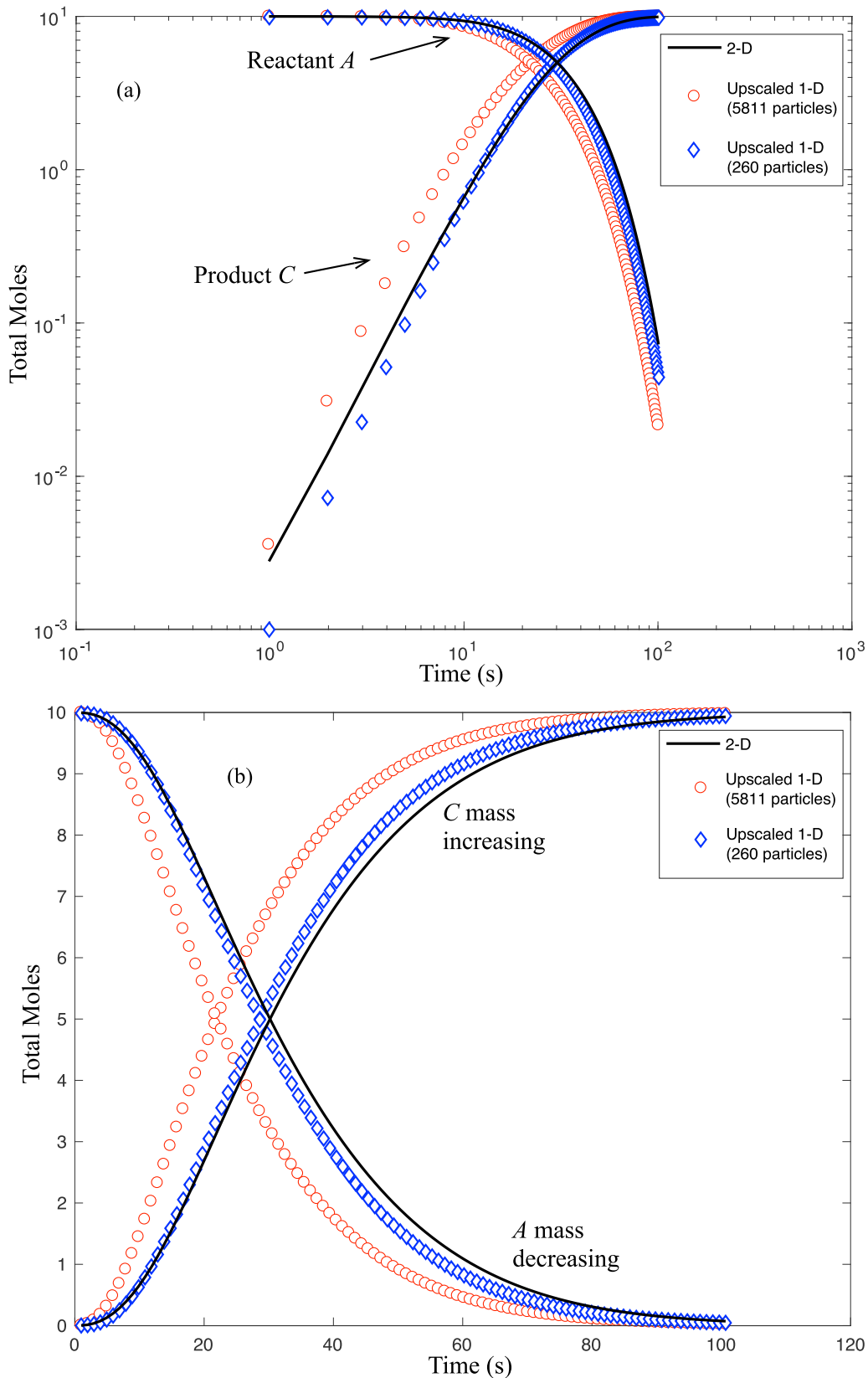


Fig. 4. Log-log (a) and linear (b) plots of total domain moles of reactant *A* and product *C* in both the 2-D full velocity model (red curves) and 1-D upscaled (single velocity) model (blue circles). Upscaled 1-D model uses local $D_{mol} = 10^{-3} \text{ mm}^2/\text{s}$ for inter-particle mixing and Taylor hydrodynamic dispersion $D_{mac} = D_{eff}(t) = 4.8(1 - \exp(-t/25s)) \text{ mm}^2/\text{s}$ for random-walk particle spreading. (For interpretation of the references to colour in this figure legend, the reader is referred to the web version of this article.)

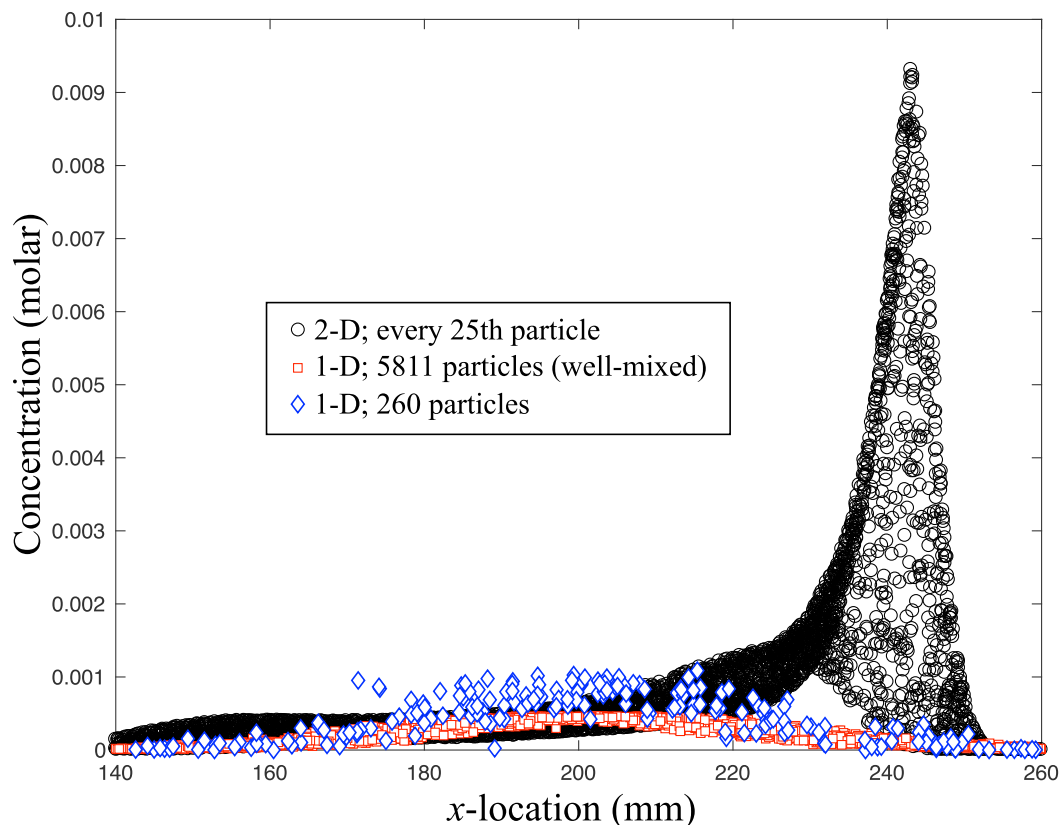


Fig. 5. Particle concentrations at a dimensionless time $t/t_D = 0.1$ with $t_D = b^2/D_{mol} = 1000s$ for single realizations of 1) a 260,000-particle 2-D model (black circles); 2) a 5,811-particle upscaled 1-D model (red squares); and, 3) a 260-particle upscaled 1-D model (blue diamonds). (For interpretation of the references to colour in this figure legend, the reader is referred to the web version of this article.)

volume, or average spacing, in 1-D is defined by $\Delta s = (5 \times 10^{-4})^{1/2} = 0.0224$ mm. Therefore, for the 10 mm initial condition for reactant A, an equivalently well-mixed 1-D model would use $N = 10 \text{ mm}/0.0224 \text{ mm} = 447$. The total particle number including the surrounding initial B reactant is 5811. Upon upscaling, however, the concentrations are not locally well-mixed. The projection to 1-D places disparate concentrations in the same x -location. The particles may represent these different concentrations, and do so by representing some support volume. This volume has been shown (Paster et al., 2014; Schmidt et al., 2017) to represent the concentration auto-correlation (and as time grows, the cross-correlation) distance. Previous studies (e.g., Kapoor et al., 1997) have shown that, in Poiseuille flow, the reactants segregate in regions that occupy about one-half the width of the aperture. This is verified in Fig. 2a. Therefore, each particle occupies a 1-D volume upon upscaling of ≈ 0.5 mm. This gives an initial particle number of 20 for the A initial condition, or 260 total particles. This visual estimate is formally shown to be representative in the Appendix. These particle numbers (5811 and 260, for well-mixed and segregated) were placed in a 1-D model using a newer particle-tracking algorithm (Benson and Bolster, 2016; Schmidt et al., 2018a). For the lower number, we also used an ensemble of 100 simulations due to noisy runs.

This newer algorithm (Benson and Bolster, 2016; Schmidt et al., 2018a) transfers masses or moles of any and all species (denoted by a superscript, i.e., species A as m^A) during a time-step of duration Δt between all particle pairs i and j (denoted by subscripts) according to

$$m_j^A(t + \Delta t) = m_j^A(t) + \sum_i \frac{1}{2} (m_i^A(t) - m_j^A(t)) P_{i,j}, \quad (2)$$

using each particle pair's collocation probability

$$P_{i,j} = (\Delta s / \sqrt{8\pi\eta D_{mol}\Delta t}) \exp(-r^2 / (8\eta D_{mol}\Delta t)), \quad (3)$$

where Δs is the particle support volume, r is the distance between the i and j particles, and $0 < \eta < 1$ is the fraction of the isotropic diffusion simulated by interparticle mass transfer. Because the mass transfer process is diffusive (Schmidt et al., 2018a), any “leftover” diffusion is added to macro-dispersion, i.e., by $(1 - \eta)D_{mol} + D_{mac}$, which is simulated by random walks (Benson and Bolster, 2016). We chose $\eta = 1/2$, although it makes no observable difference as long as the value is not extremely close to 0 or 1. Note that Δs is essentially calculated automatically as for any j , the probabilities must satisfy $\sum_i P_{i,j} = 1$; therefore, a matrix of probabilities is adjusted to have a column sum of unity (see Schmidt et al., 2018a). Also, the masses in the sum can be from the beginning or end of a time-step, or updated sequentially (Schmidt et al., 2018a). We chose the sequential updating here for stability. After mass transfer of A and B among all particles, the bimolecular reaction proceeds according to a first-order implementation of the law of mass action (Benson and Bolster, 2016), namely

$$\Delta m_j^A = \Delta m_j^B = -\Delta m_j^C = -k\Delta t \Delta s (m_j^A / \Delta s)(m_j^B / \Delta s). \quad (4)$$

After mass transfer and reaction, the particles experience advection and any additional local and macro-dispersion by well-known random walk methods (Labolle et al., 1996; Salamon et al., 2006). Specifically, in the 2-D model, particles are advected by $v_x(y)\Delta t$ and isotropically diffused by $(1 - \eta)D_{mol}$, while the 1-D models advect by $\bar{v}\Delta t$ and disperse using Taylor's $(1 - \eta)D_{mol} + D_{mac}(t)$ unless otherwise specified for hypothesis testing.

3. Results and discussion

The rates of C production and late-time A decline agree quite well in both log-log and linear coordinates, when the lower number of initial A particles ($N = 260$) is used to represent concentration fluctuation

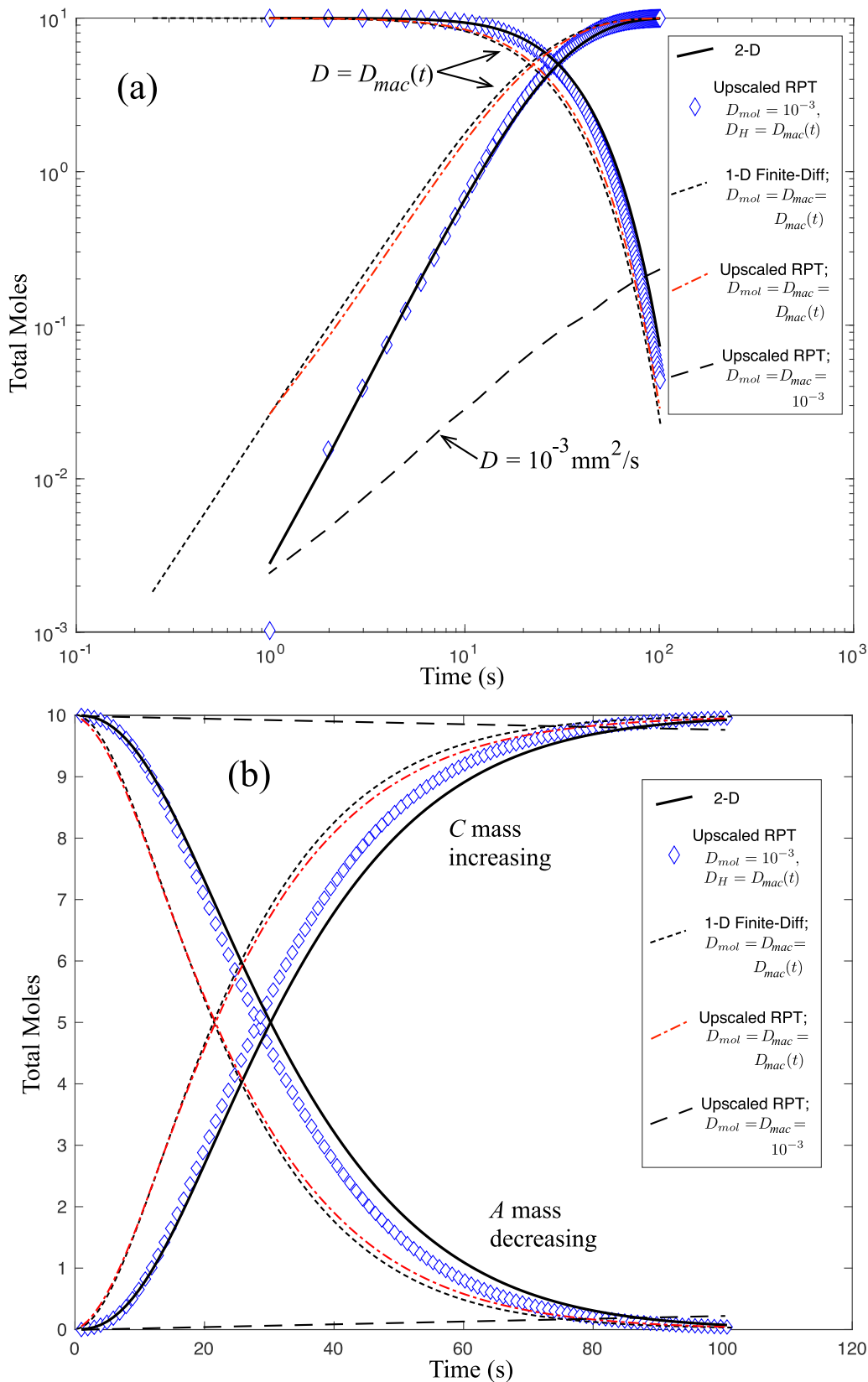


Fig. 6. Log-log (a) and linear (b) plots of total domain moles of reactant A (decreasing) and product C (increasing) in both the 2-D full velocity model (black solid curves) and the 1-D upscaled (single velocity) models. Blue diamond symbols are the previous model using local $D_{mol} = 10^{-3} \text{ mm}^2/\text{s}$ for inter-particle mixing and Taylor hydrodynamic dispersion $D_{mac} = D_{eff}(t) = 4.88(1 - \exp(-t/25s)) \text{ mm}^2/\text{s}$ for random-walk particle spreading. Black dashed (finite-difference model) and red dot-dash (RPT model) curves use $D_{eff}(t)$ for both mixing and spreading, black wide dashed curves use D_{mol} for both in RPT model. (For interpretation of the references to colour in this figure legend, the reader is referred to the web version of this article.)

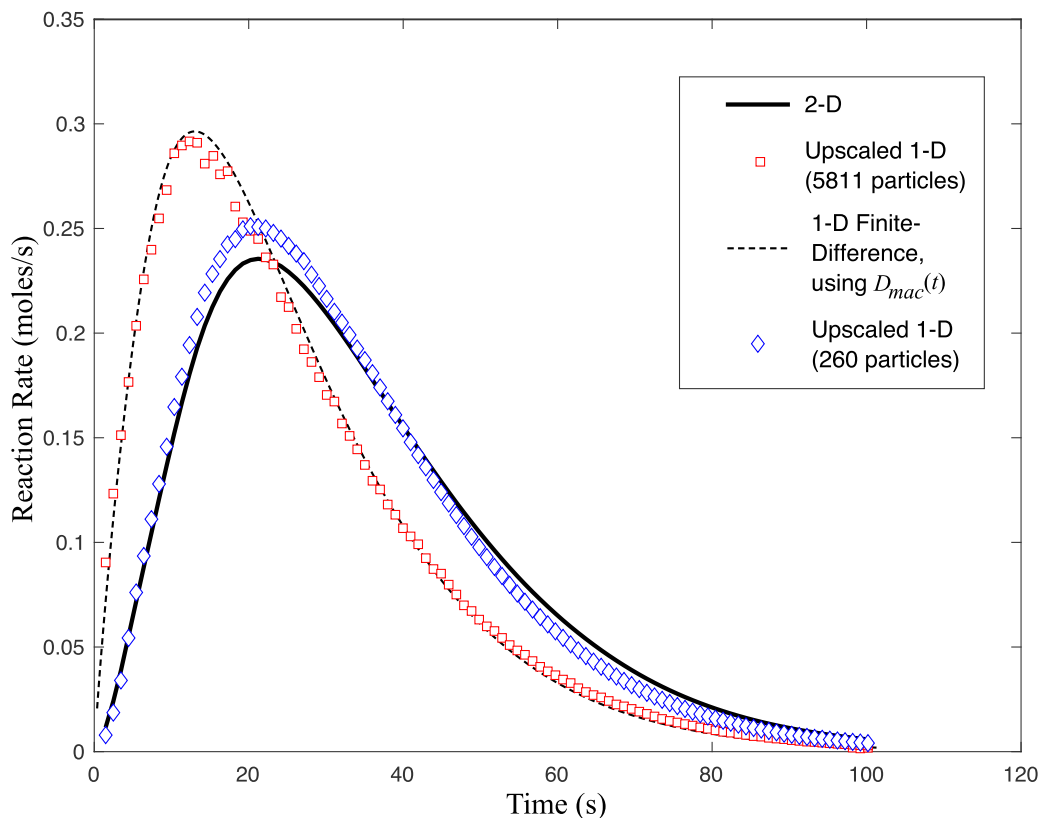


Fig. 7. Total reaction rates in full 2-D simulation (solid black curve) and upscaled 1-D models. The dashed black line is a finite-difference model with $D = D_{eff}(t)$, the red squares represent an RPT model with 447 initial A (5811 total) particles, and the blue diamonds use 20 initial A (260 total) particles. (For interpretation of the references to colour in this figure legend, the reader is referred to the web version of this article.)

distances on the order of one-half pore width (Fig. 4). We expect that an even better fit could be achieved by adjusting the particle number, but we have not changed our original visual estimate of particle support volume equal to one-half pore width (see also the appendix). This level of agreement was not expected due to the loss of detailed velocity information upon upscaling. By virtue of a constant velocity and Gaussian random walks, the 1-D model has a Gaussian shape at any time. The fact that the shape of the “plume” appears to be of secondary importance would indicate that the magnitude of concentration fluctuations, along with the rate at which these fluctuations mix at the local scale, is a primary driver of reaction rate (see also Tartakovsky and Barajas-Solano, 2018).

We can inspect the degree to which different concentrations coexist in close proximity by examining a plot of each particle’s concentration of A versus position along the x-axis in both the 2-D and 1-D RPT models (Fig. 5). These concentrations are given by dividing the species masses by particle support volume Δs . For clarity we plot every 25th particle from the 260,000 initial A particle model in 2-D, along with single realizations from the 5811 particle and 260 particle models in 1-D, all at a time of 100 s ($=t_D/10$). Unlike an Eulerian model, the 1-D upscaled models have particles at, or near, the same position with very different concentrations. This happens because the properly upscaled dispersive random walks take particles with different masses and move them relatively large distances, using $D_{mac}(t)$, into areas of very different concentrations. The local transfer of mass between particles takes place more slowly than this (according to D_{mol}), so there is not enough time to equilibrate with surroundings before a new excursion. This is especially true in the 260-particle model, and shows that a key to this upscaling is a correct calculation of the large-scale excursion lengths versus the local-scale mixing rate. Also evident in Fig. 5 is that the 1-D model has lost information about the particular velocity distribution and performs Gaussian random walks.

A more important point is the difference between the Lagrangian model with mixing given by $D = 10^{-3}$ mm²/s and spreading by $D_{mac}(t)$, and an Eulerian model that uses the same value (either D_{mol} or $D_{mac}(t)$) for both mixing and dispersion. We ran the 1-D models using these potential end-member choices for mixing and dispersion, and found that those upscaled models under-predict and over-predict reaction magnitudes significantly (Fig. 6). This is further emphasized by a plot of the global reaction rates (Fig. 7). To check the accuracy of these particle models, we also coded a 1-D Eulerian model using upwind finite-differences (FD) and $D_{mac}(t)$. With a constant velocity and Courant number of unity, the FD model does not suffer numerical dispersion, and it verifies the RPT model using upscaled single valued $D = D_{mac}(t)$. This model using $D_{mac}(t)$ for both mixing and spreading is a better model than using D_{mol} for both, which indicates that it is more important for the reactants to be placed in the proper positions before mixing begins, even if the local mixing is overdone. That is why, for $t \rightarrow 0$, the reactant initial condition specifies the correct positions and using D_{mol} is the better model. After a time of approximately $t_D/10$, the solute, if placed in the proper positions, becomes better-mixed and using D_{mac} is more appropriate (see Cirpka and Kitanidis, 2000a; Dentz and Carrera, 2007; Porta et al., 2012), if one is forced to use a deterministic Eulerian model. However, in the next section we will see that an effective, intermediate value $D_{mol} \leq D_{eff} \leq D_{mac}$ is better still.

3.1. Analytic/semi-analytic upscaling

As discussed in the Introduction, two forms of upscaling have been derived and/or suggested for the mixing versus spreading problem. One extends the approach of Porta et al. (2012), who volume-average the reactive transport equations. Those authors solve for the asymptotic ($t \rightarrow \infty$) coefficients in upscaled equations that keep first-order terms only. We extend their approach for coefficients that are functions of

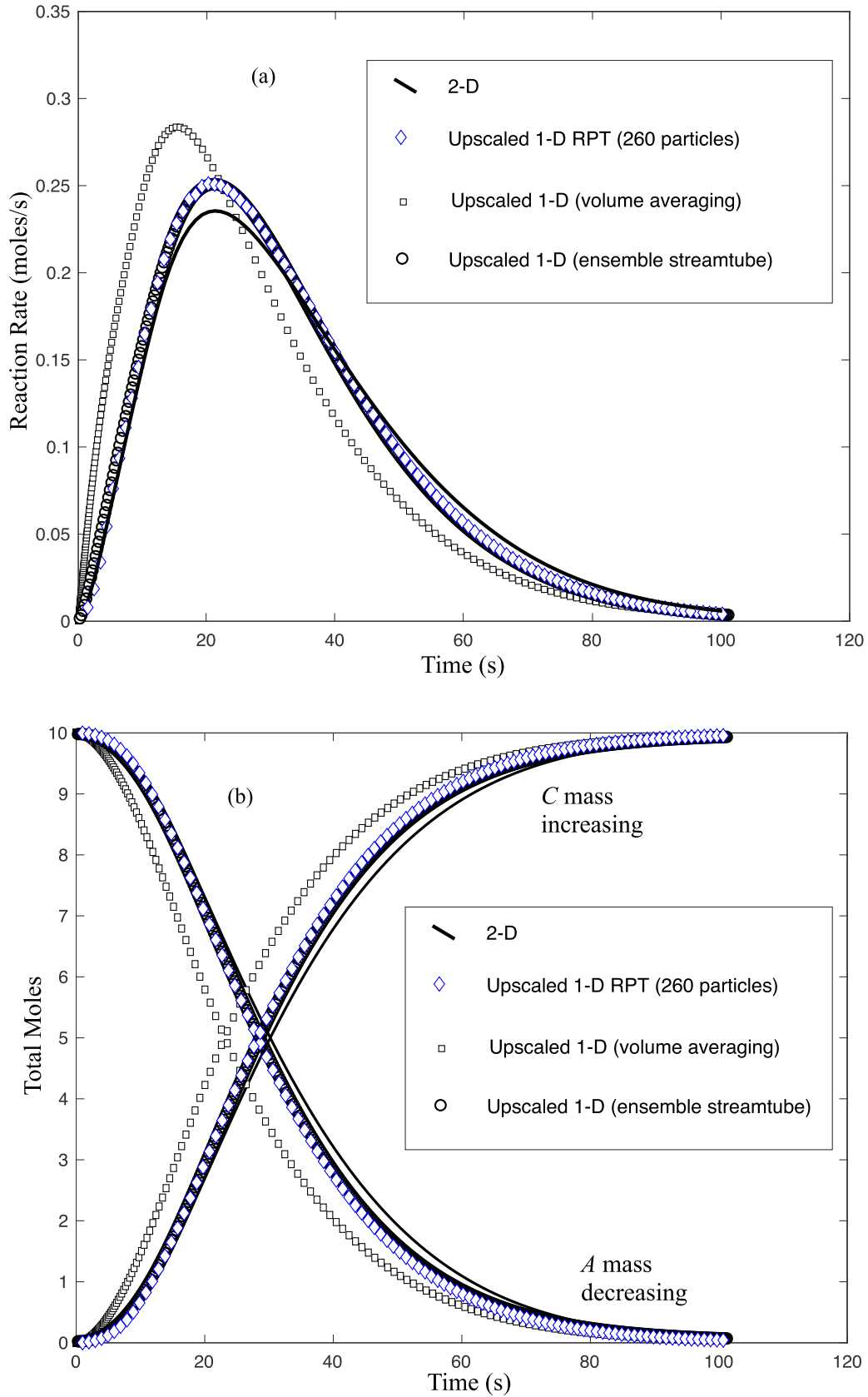


Fig. 8. Results from the simulated upscaled 1-D equations: (a) Total reaction rates and (b) Total simulated domain moles of reactant A and product C. Black squares are volume-averaged equations (23) through (35). Black circles are stream-tube model using $D_{eff}(t)$ in (1). Previously plotted results for the full 2-D and 260 initial A-particle 1-D models are included for reference. The streamtube model results are almost completely obscured by the 260 particle model results.

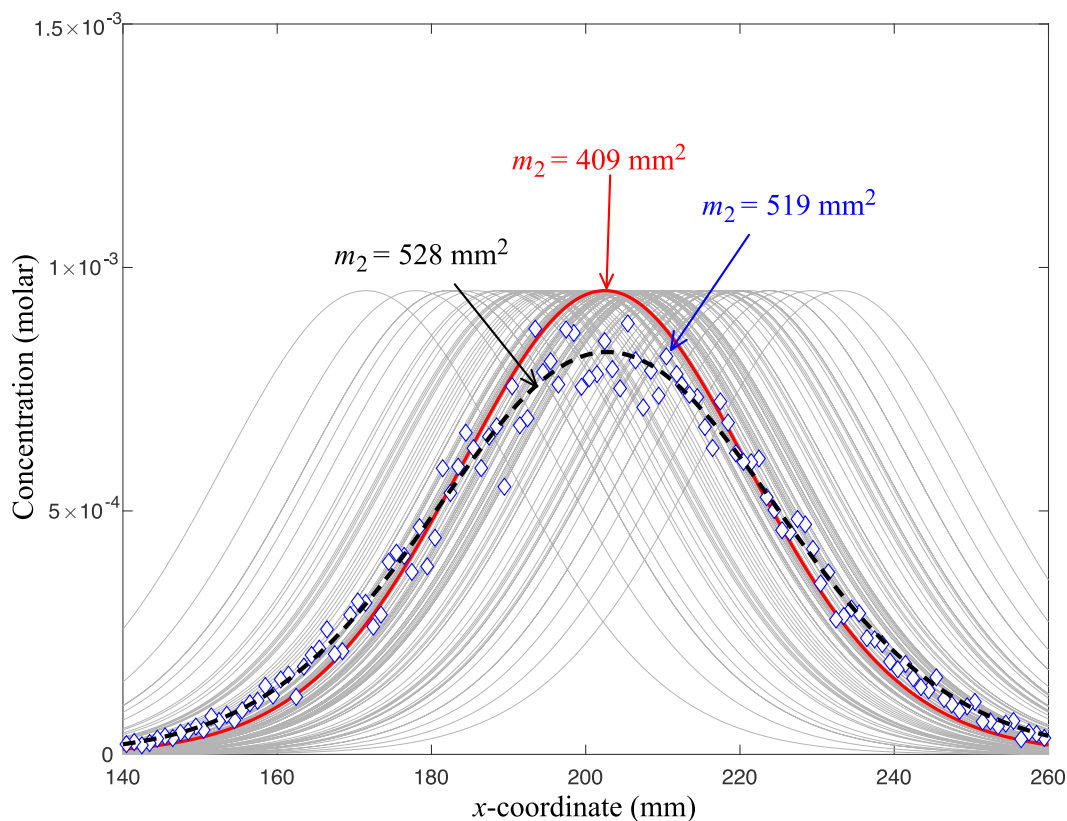


Fig. 9. Concentrations of reactant A versus x -coordinate at time $t_D/10 \approx 100$ s in upscaled models: Solid red curve is 1-D finite-difference solutions of (1) for $i = A, B, C$ using $\mathbf{D} = D_{eff}(t)$. Light grey curves are 100 random placements of the red curve with spatial variance $2t \int_0^t [D_{mac}(\tau) - D_{eff}(\tau)] d\tau$. The black dashed line is the superposition (ensemble average) of 1000 randomly placed grey curves. Blue diamond symbols are 100-realization ensemble average of the 260-particle RPT model. Calculated spatial centered second moments of model results (denoted m_2) show the close correspondence of the streamtube and ensemble particle results. (For interpretation of the references to colour in this figure legend, the reader is referred to the web version of this article.)

time (Appendix). The result is two coupled transport equations, one for a reactive species and another for the conservative species $A - B$.

A Galilean-invariant (i.e., $\bar{v} = 0$) set of these equations was solved on a finite-difference grid using centered differences for first derivatives, a classical 3-point stencil for second derivatives, and operator-splitting for reaction, so that the solution is $\mathcal{O}(\Delta x^2, \Delta t)$. Discretization was decreased until convergence was observed with a final $\Delta x = 0.1$ mm, $\Delta t = 0.001$ s. Plots of the global reaction rate, and the masses of A and C, over time (Fig. 8) show that the perturbation upscaling overpredicts the mixing and reaction rates, although the inclusion of an adjusted reaction rate in (24) improves the results relative to a simple 1-D finite difference solution of (1) using upscaled $D_{mac}(t)$ (compare Fig. 8 to Figs. 6 and 7). The full perturbation-upscaled solution shown in Fig. 8 still overpredicts reaction rates relative to the RPT solution either because of the neglect of higher-order moments or other terms to achieve closure. Specifically, the regime in question is defined by a moderately fast reaction rate ($Da = 10$ as defined by Kapoor et al. or $Da \approx 100$ by Porta's definition), which is assumed to be infinite in order for (18) to reduce to (19).

A second method (called the “streamtube-approach” by Cirpka et al.) derives two upscaled dispersion coefficients for a conservative tracer: one for effective mixing within a theoretically isolated streamtube (D_{eff}) and another for the spreading that includes the separation of the centers of mass from different velocities among the streamtubes (D_{mac}) (Cirpka and Kitanidis, 2000a, 2000b; Dentz and Carrera, 2007; Dentz et al., 2000). Actual streamtubes allow mass transfer between each other; this process promotes mixing. Therefore, the derivation of the effective diffusion within an isolated (1-d) streamtube must include the effects of cross-streamtube mixing that is lost (see the Appendix). A practical application

of this method requires solving the reactive system of transport equations (1) using D_{eff} and mapping those solutions to the positions of the streamtubes. At time t , the centers of mass have advected to a mean position of $\bar{v}t$ and accumulated some extra spreading. We may adopt the up-scaled (and Gaussian) approximation of the extra spreading by using the accumulated difference $D_{\Delta}(t) = \int_0^t [D_{mac}(\tau) - D_{eff}(\tau)] d\tau$. Calculation of $D_{mac}(t)$ is already provided in the Appendix, and using the methodology in Dentz and Carrera (2007) we further calculate $(D_{mac} - D_{eff})$ as a function of time. The 1-D solution of the reactive system using $D_{eff}(t)$ has an excellent representation of the reaction rate and evolution of reactant and product moles (Fig. 8). A superposition of these 1-D solutions with random mean positions given by $\bar{v}t + \sqrt{2tD_{\Delta}(t)}\mathcal{Z}$, where \mathcal{Z} is a standard Normal yields plots very close to the ensemble RPT model using 260 particles (Fig. 9). At the time shown in Fig. 9 ($t = 100$ s = $t_D/10$), the total moles of A remaining in the ensemble streamtube and ensemble RPT models are 0.0466 and 0.0462, while the centered second moments are 528 and 519 mm^2 , respectively. We speculate that, for this moderately fast reaction ($Da = 100$), the particle method is a stochastic implementation of the streamtube method: each particle moves by mean advection and macrodispersion, but transfers mass according to 1) the local diffusive Green's function (Schmidt et al., 2018a), and 2) the covariance of concentrations given by the particle support volume. An open question is the regions of the Da , Pe and chemical sequestration parameter space under which the correspondence holds.

4. Conclusions

In this technical note we show that the RPT method can accurately simulate dimensionally upscaled transport and reaction for pre-

asymptotic times in Poiseuille flow. We used the time-dependent, up-scaled effective Taylor macro-dispersion coefficient D_{mac} for random walks and the isotropic molecular diffusion for locally diffusive mass transfer between particles. An accurate model using finite differences would require full specification of the velocity in 2-D and take tens of millions of nodes using higher-order methods and hundreds of millions for first-order methods (Benson et al., 2017). The properly up-scaled RPT model used 20 initial A (260 total) particles, and an ensemble of 100 simulations ran in minutes on a laptop PC. The volume-averaging upscaling method did not perform as well as the streamtube method with effective diffusion for the Pe and Da values selected by Kapoor et al. (1997). The streamtube and RPT methods were essentially identical for this reactive scenario. This suggests that the RPT method is performing an equivalent upscaling procedure automatically, because the particles experience the velocity perturbations as well as the local Green's function of mixing. Both of those quantities are the key elements of the streamtube approach. An interesting hypothesis is that the RPT method will succeed in upscaling regardless of the Da , Pe regime because it does not discard any terms. If true, the particle method would be not only convenient, but theoretically preferred because, at any scale above the molecular scale in moving fluids, mixing, spreading, and chemical kinetics are completely different phenomena that should be simulated as such. Furthermore, the RPT method can accommodate any velocity field (with variability in time and space) and any reactions, whether fluid/fluid as done here, or fluid/solid (Schmidt et al., 2018b). Because the success of the RPT method depends on an accurate estimate of the particle numbers (densities), which in turn encodes the concentration perturbation autocovariance, this study highlights the importance of measuring or estimating these statistics.

Acknowledgements

We thank the editor, Graham Sander, reviewers Olaf Cirpka, Giovanni Porta, and one anonymous reviewer for extremely helpful comments. This material is based upon work supported by, or in part by, the US Army Research Office under Contract/Grant number W911NF-18-1-0338. The authors were also supported by the National Science Foundation under awards EAR-1417145, DMS-1211667, DMS-1614586, EAR-1351625, EAR-1417264, EAR-1446236, and CBET-1705770.

Appendix A. Upscaling Calculations

Begin with the 2-D equations of transport and reaction at the micro-scale (1) with a total of three compounds $i = A, B$, and C , with dispersion given by local diffusion ($\mathbf{D} = D_{mol}$), reaction terms $R = -kc_Ac_B$ for $i = A = B$, and $R = kc_Ac_B$ for $i = C$. An equation for pseudo-species concentration $c_D = c_B - c_A$, given by subtracting the equation for c_A from the same for c_B , is conservative due to the cancellation of their respective reaction terms. In particular, the resulting equation for c_D is just (1) with $R = 0$.

We may decompose concentrations and the velocity field into mean and fluctuation terms

$$\begin{aligned} c_i(t, x, y) &= \bar{c}_i(t, x) + c'_i(t, x, y), \\ v_x(y) &= \bar{v} + v'_x(y), \end{aligned} \quad (5)$$

where the overbar refers to the volume average across the y -direction and the prime to the zero-mean fluctuations about the average.

A1. Two-equation volume-averaged closure

We take a perturbative approach for upscaling by volume-averaging in the y -direction. In particular, we follow Porta et al. (2012) and Bolster et al. (2011) with an extension to include time-variable upscaled coefficients. This approach discards a number of second- and higher-order moments in order to reach closure with two PDEs.

For the conservative compound, place (5) and $R = 0$ into (1)

$$\frac{\partial \bar{c}_D}{\partial t} + \frac{\partial c'_D}{\partial t} + (\bar{v} + v'_x) \left(\frac{\partial \bar{c}_D}{\partial x} + \frac{\partial c'_D}{\partial x} \right) = D_{mol} \frac{\partial^2 \bar{c}_D}{\partial x^2} + D_{mol} \nabla^2 c'_D \quad (6)$$

An average across y gives

$$\frac{\partial \bar{c}_D}{\partial t} + \bar{v} \frac{\partial \bar{c}_D}{\partial x} = D_{mol} \frac{\partial^2 \bar{c}_D}{\partial x^2} - \frac{\partial v'_x c'_D}{\partial x} \quad (7)$$

The closure problem for c'_D can be written by neglecting the second order term $\frac{\partial v'_x c'_D}{\partial x}$ and subsequently subtracting (7) from (6):

$$\frac{\partial c'_D}{\partial t} + \bar{v} \frac{\partial c'_D}{\partial x} + v'_x \frac{\partial \bar{c}_D}{\partial x} = D_{mol} \nabla^2 c'_D. \quad (8)$$

Following Porta (Porta et al., 2012), we assume that

$$c'_D = p \frac{\partial \bar{c}_D}{\partial x} \quad (9)$$

which, when plugged into (8) and assuming that transverse processes are most important, implies that $p = p(y, t)$ satisfies

$$\frac{\partial p}{\partial t} + v' = D_{mol} \frac{\partial^2 p}{\partial y^2}. \quad (10)$$

The solution of this boundary-value problem is

$$p(y, t) = - \int_0^t \int_0^b v'(\eta) G(y, t - \tau | \eta) d\eta d\tau \quad (11)$$

where G is the transverse diffusion Green's function, namely

$$G(y, t, \eta) = \frac{1}{b} + \frac{2}{b} \sum_{n=1}^{\infty} \cos\left(\frac{n\pi y}{b}\right) \cos\left(\frac{n\pi \eta}{b}\right) \exp\left(-\frac{D_{mol} n^2 \pi^2 t}{b^2}\right). \quad (12)$$

Thus,

$$p(y, t) = \sum_{n=1}^{\infty} \frac{12b^2 \bar{v}}{D_{mol} n^4 \pi^4} \cos\left(\frac{n\pi y}{b}\right) \left[1 - \exp\left(-\frac{D_{mol} n^2 \pi^2 t}{b^2}\right) \right] \quad (13)$$

and this further implies

$$\frac{\partial v'_x c'_D}{\partial x} = -v'_x p \frac{\partial^2 \bar{c}_D}{\partial x^2} = -D_{mac}(t) \frac{\partial^2 \bar{c}_D}{\partial x^2}, \quad (14)$$

where the upscaled hydrodynamic dispersion coefficient is given by

$$D_{mac}(t) = 144 \frac{\bar{v}^2 b^2}{\pi^6 D_{mol}} \sum_{n=1}^{\infty} (1 + (-1)^n) \frac{1}{n^6} \left[1 - \exp\left(-\frac{D_{mol} n^2 \pi^2 t}{b^2}\right) \right]. \quad (15)$$

We also note that for the values of the physical problem chosen here, the first non-zero term (i.e., $n = 2$) provides a reasonable approximation

$$\begin{aligned} D_{mac}(t) &\approx \frac{9\bar{v}^2 b^2}{2\pi^6 D_{mol}} \left[1 - \exp\left(-\frac{D_{mol} 4\pi^2 t}{b^2}\right) \right] \\ &\approx 4.75 \frac{mm^2}{s} (1 - \exp(-t/25.3 \text{ s})). \end{aligned} \quad (16)$$

Note that at asymptotic times, as $t \rightarrow \infty$ the infinite series in (15) converges to $\frac{\bar{v}^2 b^2}{210 D_{mol}}$, as it must given the original derivation of Taylor dispersion originating back to Taylor (1953).

A2. Reactive compounds

Returning to the ADRE for the non-conservative compound B , averaging vertically yields the equation

$$\frac{\partial \bar{c}_B}{\partial t} + \bar{v} \frac{\partial \bar{c}_B}{\partial x} = D_{mol} \frac{\partial^2 \bar{c}_B}{\partial x^2} - \frac{\partial v'_x c'_B}{\partial x} - k \left[\bar{c}_B (\bar{c}_B - \bar{c}_D) + \overline{c'_B (c'_B - c'_D)} \right]. \quad (17)$$

To first order, the closure for c'_B is

$$\frac{\partial c'_B}{\partial t} + \bar{v} \frac{\partial c'_B}{\partial x} + v' \frac{\partial \bar{c}_B}{\partial x} = D_{mol} \nabla^2 c'_B - k \left[c'_B (\bar{c}_B - \bar{c}_D) + \bar{c}_B (c'_B - c'_D) \right]. \quad (18)$$

For fast reactions ($Da > 1$) the reaction term dominates, i.e. the right most term is larger than any other terms in the equation such that these can be neglected, meaning that the terms in the square parentheses sum to zero. As such, solving for c'_B yields

$$c'_B = \frac{\bar{c}_B}{2\bar{c}_B - \bar{c}_D} c'_D = \frac{\bar{c}_B}{2\bar{c}_B - \bar{c}_D} p(y, t) \frac{\partial \bar{c}_D}{\partial x} = M(x, t) p(y, t) \frac{\partial \bar{c}_D}{\partial x} \quad (19)$$

where the mixing ratio is

$$M(x, t) = \frac{\bar{c}_B}{2\bar{c}_B - \bar{c}_D} = \frac{\bar{c}_B}{\bar{c}_B + \bar{c}_A}.$$

Thus, we find

$$\frac{\partial v' c'_B}{\partial x} = -\bar{v}' p \frac{\partial}{\partial x} \left(M(x, t) \frac{\partial \bar{c}_D}{\partial x} \right) = -D_{mac}(t) \frac{\partial}{\partial x} \left(M(x, t) \frac{\partial \bar{c}_D}{\partial x} \right), \quad (20)$$

and using (9),

$$\overline{c'_B (c'_B - c'_D)} = \overline{M c'^2_D (M - 1)} = M(M - 1) \left(\frac{\partial \bar{c}_D}{\partial x} \right)^2 \bar{p}^2, \quad (21)$$

where

$$\bar{p}^2 = \sum_{n=1}^{\infty} \frac{144 \bar{v}^2 b^4}{D_{mol}^2 n^8 \pi^8} (1 + (-1)^n) \left[1 - 2 \exp \left(\frac{-D_{mol} n^2 \pi^2 t}{b^2} \right) + \exp \left(\frac{-2D_{mol} n^2 \pi^2 t}{b^2} \right) \right]. \quad (22)$$

Therefore, our upscaled equations are:

$$\frac{\partial \bar{c}_D}{\partial t} + \bar{v} \frac{\partial \bar{c}_D}{\partial x} = \left(D_{mol} + D_{mac}(t) \right) \frac{\partial^2 \bar{c}_D}{\partial x^2}, \quad (23)$$

$$\begin{aligned} \frac{\partial \bar{c}_B}{\partial t} + \bar{v} \frac{\partial \bar{c}_B}{\partial x} &= D_{mol} \frac{\partial^2 \bar{c}_B}{\partial x^2} + D_{mac}(t) \frac{\partial}{\partial x} \left(M(x, t) \frac{\partial \bar{c}_D}{\partial x} \right) \\ &\quad - k \left(\bar{c}_B (\bar{c}_B - \bar{c}_D) + M(M - 1) \left(\frac{\partial \bar{c}_D}{\partial x} \right)^2 K(t) \right), \end{aligned} \quad (24)$$

where

$$D_{mac}(t) = 144 \frac{\bar{v}^2 b^2}{\pi^6 D_{mol}} \sum_{n=1}^{\infty} (1 + (-1)^n) \frac{1}{n^6} \left[1 - \exp \left(\frac{-D_{mol} n^2 \pi^2 t}{b^2} \right) \right], \quad (25)$$

and

$$\begin{aligned} K(t) = \bar{p}^2 &= \sum_{n=1}^{\infty} \frac{144 \bar{v}^2 b^4}{D_{mol}^2 n^8 \pi^8} (1 + (-1)^n) \left[1 - 2 \exp \left(\frac{-D_{mol} n^2 \pi^2 t}{b^2} \right) \right. \\ &\quad \left. + \exp \left(\frac{-2D_{mol} n^2 \pi^2 t}{b^2} \right) \right]. \end{aligned} \quad (26)$$

Note that while we have generally followed (Porta et al., 2012), one difference does exist, which perhaps explains any possible discrepancies between our findings and theirs. In Porta's work they do not consider an explicit time dependent reaction coefficient as above. Later work, also by Porta et al. (2016), suggests that more complex closures can be used when coefficients are time dependent, resulting in a nonlocal integro-differential equation. However that system is significantly more computationally intensive than this closure. Additionally, the closure approximation was originally postulated strictly for cases where $Da \gg Pe$, although it was verified also for cases where $Da \gg 1$ and Pe and Da had similar values as here.

A3. Streamtube mixing model

Let us define global first, second, and second centered moments:

$$\begin{aligned} M_1(t) &= \frac{1}{b} \int_0^b \int_{-\infty}^{\infty} xc(t, x, y) dx dy \\ M_2(t) &= \frac{1}{b} \int_0^b \int_{-\infty}^{\infty} x^2 c(t, x, y) dx dy \\ K_2 &= M_2(t) - M_1^2(t). \end{aligned} \quad (27)$$

The macroscopic dispersion coefficient is half the rate of change of the second centered global moment; i.e.

$$D_{mac} = \frac{1}{2} \frac{dK_2}{dt}. \quad (28)$$

Similarly we can define local first, second, and second centered moments:

$$\begin{aligned} m_1(y, t) &= \int_{-\infty}^{\infty} xc(t, x, y) dx \\ m_2(y, t) &= \int_{-\infty}^{\infty} x^2 c(t, x, y) dx \\ \kappa_2(y, t) &= m_2(y, t) - m_1^2(y, t) \end{aligned} \quad (29)$$

With these, we can define an alternative dispersion coefficient

$$D_{eff} = \frac{1}{2} \frac{d}{dt} \left(\frac{1}{b} \int_0^b \kappa_2(y, t) dy \right), \quad (30)$$

which is a better measure of mixing than D_{mac} , which captures both mixing and spreading (Cirpka and Kitanidis, 2000b; Dentz and Carrera, 2007). Consider the difference between the first local and global moment, $p(y, t) = m_1(y, t) - M_1(t)$. It is straightforward to show that its governing equation and solution is the same as (10) such that

$$p(y, t) = \sum_{n=1}^{\infty} \frac{12b^2 \bar{v}}{D_{mol} n^4 \pi^4} \cos \left(\frac{n\pi y}{b} \right) \left[1 - \exp \left(\frac{-D_{mol} n^2 \pi^2 t}{b^2} \right) \right] \quad (31)$$

The global and local second centered moments can be related by

$$K_2(t) = \frac{1}{b} \int_0^b \kappa_2(y, t) dy + \frac{1}{b} \int_0^b p^2(y, t) dy \quad (32)$$

which means that the macroscopic and effective dispersion coefficients are related by

$$D_{mac}(t) - D_{eff}(t) = \frac{1}{2} \frac{d}{dt} \left(\frac{1}{b} \int_0^b p^2(y, t) dy \right) = \frac{1}{2} \frac{d\bar{p}^2}{dt} \quad (33)$$

Using (10) gives

$$\begin{aligned} D_{mac}(t) - D_{eff}(t) &= \sum_{n=1}^{\infty} \frac{144 \bar{v}^2 b^2}{D_{mol} n^6 \pi^6} ((1 + (-1)^n) \\ &\quad \times \left[\exp \left(\frac{-D_{mol} n^2 \pi^2 t}{b^2} \right) - \exp \left(\frac{-2D_{mol} n^2 \pi^2 t}{b^2} \right) \right] \end{aligned} \quad (34)$$

To leading order,

$$\begin{aligned} D_{mac}(t) - D_{eff}(t) &\approx \frac{9\bar{v}^2 b^2}{2\pi^6 D_{mol}} \left[\exp \left(\frac{-4D_{mol} \pi^2 t}{b^2} \right) - \exp \left(\frac{-8D_{mol} \pi^2 t}{b^2} \right) \right] \end{aligned} \quad (35)$$

A4. Particle numbers

The number of particles used in the RPT model is based on the spatial covariance of concentrations. Mixing in the Poiseuille system is dominated by transverse concentration gradients, so we may examine the transverse autocovariance and reactant segregation that develops almost immediately after the initial condition is distorted by the velocity field. To our knowledge, expressions for the concentration statistics

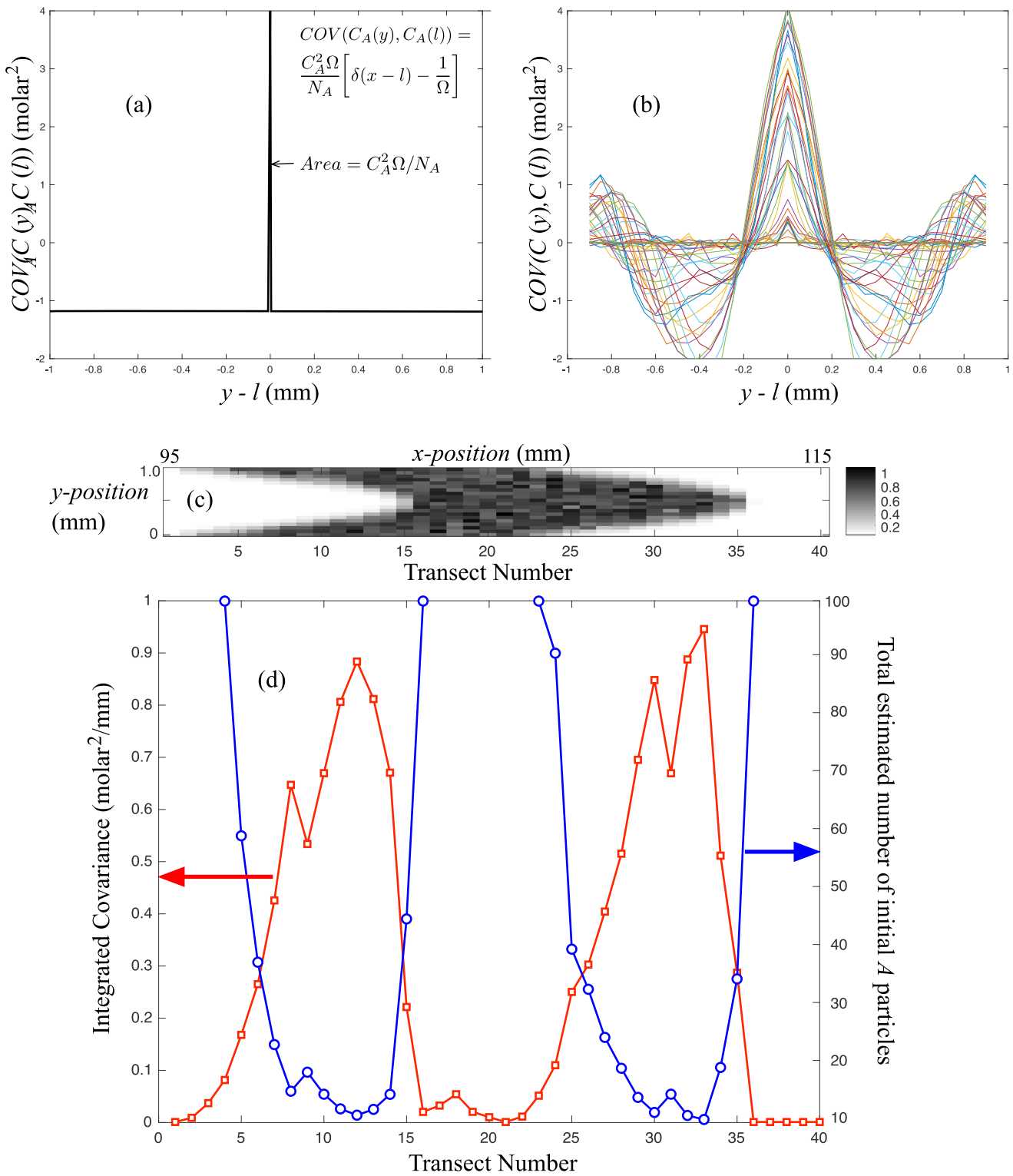


Fig. 10. (a) Plot of autocovariance function for uniformly randomly placed Dirac delta function particles in a domain of size 1 mm. (b) Calculated y-direction autocovariance for nonreactive 260,000 particle 2-D model. Functions calculated at 40 transects from $95 \leq x \leq 115$ mm. (c) Binned A concentrations from nonreactive 260,000 particle 2-D model showing locations of y-transects used in subfigure (b). (d) Red squares: Calculated integrated autocovariances (areas) from the 40 transects in the center ($y - l = 0$), positive parts of the autocovariance functions in (b), and Blue circles: calculated total initial numbers of A particles for upscaled 1-D models, based on calculated areas on the same plot.

have not been developed for the reactive system. Indeed, even the conservative system will experience dilution (and reduced total variance) as time gets large, so we look at the concentrations that develop early at a dimensionless time of $5t_A = t_D/20 = 5$ s. This ensures plenty of advective distortion but minimal dilution.

A 260,000 particle simulation was run with all parameters identical to the reactive simulation, except that the reaction rate coefficient was set to zero. At a time of 5 s, the A concentrations were binned (Fig. 10c) and the covariance functions at each of 40 y-transsects were calculated numerically (Fig. 10b). We are especially interested in the area corresponding to the positive covariance portion at small spatial separations in the center of these plots. A visual estimate of the “extent” of the A concentrations is on the order of one-half pore width (Fig. 2), which is the number we used in our uncalibrated simulations. Of course the A concentration covariance will be different along the length of the A “plume”, so we examine the variability here.

The autocovariance function (Fig. 10a) for uniformly randomly placed Dirac-delta function particles placed in a finite domain was derived by Schmidt et al. (2017):

$$COV(C_A(y), C_A(l)) = \frac{N_A m_p^2}{\Omega} \left[\delta(y-l) - \frac{1}{\Omega} \right] = C_A m_p \left[\delta(y-l) - \frac{1}{\Omega} \right], \quad (36)$$

where $C_A \approx C_A(t=0)$ is the initial, undiluted A concentration, N_A is the initial number of A particles, m_p is the mass of each particle, Ω is the extent of the domain (here 1 mm in the transverse direction), and δ is a Dirac-delta function. Several studies have shown that equating the integral of this covariance to the integral of the real covariance function makes the particle model most closely match concentration evolution in real and numerical systems with concentration segregation (Bolster et al., 2016; Ding et al., 2012; Ding et al., 2017; Paster et al., 2014; Schmidt et al., 2017). The fact that the delta particles have an atom of covariance at the origin (Fig. 10a) is not a problem as they assume a Gaussian kernel shape when the mass transfer algorithm is applied.

Integrating the covariance function means that the near-origin integrated “area” for the delta particles is $C_A m_p$. Because the particle mass is $m_p = C_A \Omega / N_A$, the area can be written $C_A^2 \Omega / N_A$ (with units $[C^2 L]$). Equating this to the numerically estimated near-origin area (with units $[C^2 L]$) gives a particle density $N_A / \Omega = C_A^2 / \text{Area} = 1 \text{ Mol}^2 / \text{Area}$. This number is particles per mm in the y-direction. The initial condition here is 10 mm in the x-direction, so the total number of initial A particles is $10 \times$ the density. A plot of the near-origin areas and the resultant total number of A particles (Fig. 10d) shows that the number ranges from 11 to 40 in the high-mixing regions, with an average of 21, supporting our visual estimate of 20 for the initial condition. It may well be that a lower number would give an even better, i.e., slightly slower mixing, model, but we have not performed any calibration.

Supplementary material

Supplementary material associated with this article can be found, in the online version, at doi:10.1016/j.advwatres.2018.11.001

References

- Benson, D.A., Aquino, T., Bolster, D., Engdahl, N., Henri, C.V., Fernández-García, D., 2017. A comparison of Eulerian and Lagrangian transport and non-linear reaction algorithms. *Adv. Water Resour.* 99, 15–37. <https://doi.org/10.1016/j.advwatres.2016.11.003>.
- Benson, D.A., Bolster, D., 2016. Arbitrarily complex chemical reactions on particles. *Water Resour. Res.* 52 (11), 9190–9200. <https://doi.org/10.1002/2016WR019368>.
- Benson, D.A., Meerschaert, M.M., 2008. Simulation of chemical reaction via particle tracking: diffusion-limited versus thermodynamic rate-limited regimes. *Water Resour. Res.* 44, W12201. <https://doi.org/10.1029/2008WR007111>.
- Bolster, D., de Anna, P., Benson, D.A., Tartakovsky, A.M., 2012. Incomplete mixing and reactions with fractional dispersion. *Adv. Water Resour.* 37, 86–93.
- Bolster, D., Paster, A., Benson, D.A., 2016. A particle number conserving Lagrangian method for mixing-driven reactive transport. *Water Resour. Res.* 52 (2), 1518–1527. <https://doi.org/10.1002/2015WR018310>.
- Bolster, D., Valdés-Parada, F.J., LeBorgne, T., Dentz, M., Carrera, J., 2011. Mixing in confined stratified aquifers. *J. Contam. Hydrol.* 120, 198–212.

- Brantley, S.L., Kubicki, J.D., White, A.F. (Eds.), 2008. *Kinetics of Water-Rock Interaction*. Springer-Verlag New York.
- Cirpka, O.A., Kitanidis, P.K., 2000. An advective-dispersive stream tube approach for the transfer of conservative-tracer data to reactive transport. *Water Resour. Res.* 36 (5), 1209–1220. <https://doi.org/10.1029/1999WR900355>.
- Cirpka, O.A., Kitanidis, P.K., 2000. Characterization of mixing and dilution in heterogeneous aquifers by means of local temporal moments. *Water Resour. Res.* 36 (5), 1221–1236. <https://doi.org/10.1029/1999WR900354>.
- Dankwerts, P., 1953. Continuous flow systems: distribution of residence times. *Chem. Eng. Sci.* 2 (1), 1–13. [https://doi.org/10.1016/0009-2509\(53\)80001-1](https://doi.org/10.1016/0009-2509(53)80001-1).
- De Simoni, M., Carrera, J., Sánchez-Vila, X., Guadagnini, A., 2005. A procedure for the solution of multicomponent reactive transport problems. *Water Resour. Res.* 41 (11). <https://doi.org/10.1029/2005WR004056>.
- Dentz, M., Borgne, T.L., Englert, A., Bijeljic, B., 2011. Mixing, spreading and reaction in heterogeneous media: a brief review. *J. Contam. Hydrol.* 120–121, 1–17. *Reactive Transport in the Subsurface: Mixing, Spreading and Reaction in Heterogeneous Media*. doi: 10.1016/j.jconhyd.2010.05.002.
- Dentz, M., Carrera, J., 2007. *Mixing and spreading in stratified flow*. *Phys. Fluids* 19, 017107.
- Dentz, M., Kinzelbach, H., Attinger, S., Kinzelbach, W., 2000. Temporal behavior of a solute cloud in a heterogeneous porous medium: 1. point-like injection. *Water Resour. Res.* 36 (12), 3591–3604. <https://doi.org/10.1029/2000WR900162>.
- Ding, D., Benson, D., Paster, A., Bolster, D., 2012. Modeling bimolecular reactions and transport in porous media via particle tracking. *Adv. Water Resour.* 53, 56–65. <https://doi.org/10.1016/j.advwatres.2012.11.001>.
- Ding, D., Benson, D.A., Fernández-García, D., Henri, C.V., Hyndman, D.W., Phanikumar, M.S., Bolster, D., 2017. Elimination of the reaction rate “scale effect”: application of the Lagrangian reactive particle-tracking method to simulate mixing-limited, field-scale biodegradation at the Schoolcraft (MI, USA) site. *Water Resour. Res.* <https://doi.org/10.1002/2017WR021103>.
- Donado, L., Sánchez-Vila, X., Dentz, M., Carrera, J., Bolster, D., 2009. Multicomponent reactive transport in multicontinuum media. *Water Resour. Res.* 45, W11402. <https://doi.org/10.1029/2008WR006823>.
- Ederly, Y., Scher, H., Berkowitz, B., 2009. Modeling bimolecular reactions and transport in porous media. *Geophys. Res. Lett.* 36 (2), L02407. <http://dx.doi.org/10.1029/2008GL036381>.
- Ederly, Y., Scher, H., Berkowitz, B., 2010. Particle tracking model of bimolecular reactive transport in porous media. *Water Resour. Res.* 46 (7), W07524. <http://dx.doi.org/10.1029/2009WR009017>.
- Gramling, C., Harvey, C., Meigs, L., 2002. Reactive transport in porous media: a comparison of model prediction with laboratory visualization. *Environ. Sci. Technol.* 36 (11), 2508–2514. <https://doi.org/10.1021/es0157144>.
- Hill, J.C., 1976. Homogeneous turbulent mixing with chemical reaction. *Annu. Rev. Fluid Mech.* 8, 135–161.
- Kapoor, V., Gelhar, L.W., Miralles-Wilhelm, F., 1997. Bimolecular second-order reactions in spatially varying flows: segregation induced scale-dependent transformation rates. *Water Resour. Res.* 33 (4), 527–536. <http://dx.doi.org/10.1029/96WR03687>.
- Kapoor, V., Jafvert, C.T., Lyn, D.A., 1998. Experimental study of a bimolecular reaction in Poiseuille flow. *Water Resour. Res.* 34 (8), 1997–2004. <https://doi.org/10.1029/98WR01649>.
- Labolle, E.M., Fogg, G.E., Tompson, A.F.B., 1996. Random-walk simulation of transport in heterogeneous porous media: local mass-conservation problem and implementation methods. *Water Resour. Res.* 32 (3), 583–593.
- Le Borgne, T., Dentz, M., Villerman, E., 2013. Stretching, coalescence, and mixing in porous media. *Phys. Rev. Lett.* 110 (20), 204501. <https://doi.org/10.1103/PhysRevLett.110.204501>.
- Le Borgne, T., Ginn, T.R., Dentz, M., 2014. Impact of fluid deformation on mixing-induced chemical reactions in heterogeneous flows. *Geophys. Res. Lett.* 41 (22), 7898–7906. <https://doi.org/10.1002/2014GL062038>.
- Lehwal, A., Janiga, G., Thévenin, D., Zähringer, K., 2012. Simultaneous investigation of macro- and micro-mixing in a static mixer. *Chem. Eng. Sci.* 79 (0), 8–18. <https://doi.org/10.1016/j.ces.2012.05.026>.
- Molz, F., Widdowson, M., 1988. Internal inconsistencies in dispersion-dominated models that incorporate chemical and microbial kinetics. *Water Resour. Res.* 24, 615–619.
- Nauman, E., Buffham, B., 1983. *Mixing in continuous flow systems*. John Wiley and Sons, New Jersey.
- Paster, A., Bolster, D., Benson, D.A., 2014. Connecting the dots: semi-analytical and random walk numerical solutions of the diffusion–reaction equation with stochastic initial conditions. *J. Comput. Phys.* 263, 91–112. <https://doi.org/10.1016/j.jcp.2014.01.020>.
- Porta, G., Ceriotti, G., Thovert, J.-F., 2016. Comparative assessment of continuum-scale models of bimolecular reactive transport in porous media under pre-asymptotic conditions. *J. Contam. Hydrol.* 185–186, 1–13. <https://doi.org/10.1016/j.jconhyd.2015.12.003>.
- Porta, G.M., Chaynikov, S., Thovert, J.-F., Riva, M., Guadagnini, A., Adler, P.M., 2013. Numerical investigation of pore and continuum scale formulations of bimolecular reactive transport in porous media. *Adv. Water Resour.* 62, Part B, 243–253. <https://doi.org/10.1016/j.advwatres.2013.09.007>.
- Porta, G.M., Thovert, J.-F., Riva, M., Guadagnini, A., Adler, P.M., 2012. Microscale simulation and numerical upscaling of a reactive flow in a plane channel. *Phys. Rev. E* 86 (3), 036102–, doi: 10.1103/PhysRevE.86.036102
- Raje, D., Kapoor, V., 2000. Experimental study of bimolecular reaction kinetics in porous media. *Environ. Sci. Tech.* 34 (7), 1234–1239.
- Rezaei, M., Sanz, E., Raelis, E., Ayora, C., Vázquez-Suñé, E., Carrera, J., 2005. Reactive transport modeling of calcite dissolution in the fresh-salt water mixing zone. *J. Hydrol. (Amst.)* 311 (1), 282–298. <https://doi.org/10.1016/j.jhydrol.2004.12.017>.

- Salamon, P., Fernández-García, D., Gómez-Hernández, J.J., 2006. A review and numerical assessment of the random walk particle tracking method. *J. Contam. Hydrol.* 87 (3–4), 277–305. <https://doi.org/10.1016/j.jconhyd.2006.05.005>.
- Sánchez-Vila, X., Fernández-García, D., Guadagnini, A., 2010. Interpretation of column experiments of transport of solutes undergoing an irreversible bimolecular reaction using a continuum approximation. *Water Resour. Res.* 46, W12510.
- Schmidt, M.J., Pankavich, S., Benson, D.A., 2017. A kernel-based Lagrangian method for imperfectly-mixed chemical reactions. *J. Comput. Phys.* 336, 288–307. <https://doi.org/10.1016/j.jcp.2017.02.012>.
- Schmidt, M.J., Pankavich, S.D., Benson, D.A., 2018. On the accuracy of simulating mixing by random-walk particle-based mass-transfer algorithms. *Adv. Water Resour.* <https://doi.org/10.1016/j.advwatres.2018.05.003>. –
- Schmidt, M.J., Pankavich, S.D., Navarre-Sitchler, A., Benson, D.A., 2018. A Lagrangian method for reactive transport with solid/aqueous chemical phase interaction. <https://arxiv.org/abs/1805.06072>.
- Tartakovsky, A.M., de Anna, P., Le Borgne, T., Balter, A., Bolster, D., 2012. Effect of spatial concentration fluctuations on non-linear reactions in diffusion-reaction systems. *Water Resour. Res.* 48, W02526.
- Tartakovsky, A. M., Barajas-Solano, D., 2018. Persistent incomplete mixing in reactive flows. <https://arxiv.org/abs/1803.06693v1>.
- Taylor, G., 1953. Dispersion of soluble matter in solvent flowing slowly through a tube. *Proc. Royal Soc. London A* 219 (1137), 186–203. <https://doi.org/10.1098/rspa.1953.0139>.
- White, A.F., Peterson, M.L., 1990. Role of Reactive-Surface-Area Characterization in Geochemical Kinetic Models. *ACS Publ.*, pp. 461–475 doi:10.1021/bk-1990-0416.ch035.
- Zhang, Y., Papelis, C., 2011. Particle-tracking simulation of fractional diffusion-reaction processes. *Phys. Rev. E* 84, 066704.